A New Description of Small-Scale and Large-Scale Roughness in the Fast Ocean Surface Emissivity Model

SANG-MOO LEE[a,b,c] AND BYUNG-JU SOHN[a,d]

[a] *School of Earth and Environmental Sciences, Seoul National University, Seoul, South Korea*
[b] *NOAA–CU Center for Environmental Technology, Electrical, Computer, and Energy Engineering, University of Colorado Boulder, Boulder, Colorado*
[c] *National Snow and Ice Data Center, Cooperative Institute for Research in Environmental Sciences, University of Colorado Boulder, Boulder, Colorado*
[d] *Key Laboratory for Aerosol–Cloud–Precipitation, China Meteorological Administration, School of Atmospheric Physics, Nanjing University of Information Science and Technology, Nanjing, China*

(Manuscript received 6 May 2020, in final form 16 November 2020)

ABSTRACT: The widely used Fast Microwave Ocean Surface Emissivity Model (FASTEM) does not include the interaction between small-scale and large-scale roughness, which seems to induce errors in the ocean surface emissivity estimation. In this study, we attempt to develop a new model that might be included in the FASTEM-like model. In the developed model, the large-scale roughness is expressed as a function of the local incidence angle (LIA) within the context of Fresnel reflection theory, incorporating the interactions between the small-scale and large-scale roughness into the fast ocean surface emissivity model, as done in the two-scale approach. With the new expression of the large-scale roughness, we also provide a more physically based form of the equation for the fast ocean surface emissivity calculation that includes the small-scale scattering over a geometrically rough surface. In addition, an algorithm for estimating two-scale roughness from the measured or modeled polarized emissivities in conjunction with the proposed fast ocean surface emissivity equation is provided. The results demonstrate that the interactions between two-scale roughness should be considered in order to estimate accurate two-scale roughness influences on the ocean surface emissivity.

KEYWORDS: Ocean; Sea/ocean surface; Wind; Radiative transfer; Microwave observations; Ocean models; Waves; oceanic; Satellite observations

1. Introduction

Precise modeling of the emissivity over a wind-roughened ocean surface is important in the microwave remote sensing of ocean parameters, such as ocean surface wind speed and ocean surface salinity. The wind-generated ocean waves influence the surface emissivity through the interactions between gravity–capillary (small-scale) ocean surface waves and microwave radiation (Yueh 1997; Johnson 2006; Liu et al. 2011). Large-scale ocean surface gravity waves induce tilted facets that modify the incident angles on the ocean's surface (Gasiewski and Kunkee 1994). The whitecaps, i.e., the air–sea mixtures caused by the breaking of the ocean surface waves, also contribute to the variation in the ocean surface emissivity, because the dielectric properties of air and ocean water differ substantially (Stogryn 1972; Monahan and O'Muircheartaigh 1986; Anguelova 2008; Hwang 2012).

In general, there are two types of microwave ocean surface emissivity models resolving the surface roughness; the geometric optics approach for high frequencies and the small-perturbation method for low frequencies (Gasiewski and Kunkee 1994; Johnson 2006). To integrate two methods, the "two-scale ocean surface emissivity model" approach has been adopted. This approach is based on the geometric optics model for large-scale waves with bistatic scattering coefficients for full-Stokes's components, instead of the direct use of Fresnel reflection coefficients (Wentz 1975; Yueh 1997; Johnson 2006). However, this model demands large computational resources, hampering its practical use for remote sensing and for data assimilation in numerical weather prediction (Liu et al. 2011).

To overcome disadvantages of the two-scale model, the Met Office developed the Fast Microwave Ocean Surface Emissivity Model (FASTEM), which has been widely used for estimating the ocean surface emissivity (English and Hewison 1998; Liu et al. 2011; Bormann et al. 2012). The FASTEM incorporated a full accuracy of the rigorous two-scale models but treated small-scale and large-scale roughness influences on the ocean surface emissivity separately, to generate a fast code. In the FASTEM, the Fresnel reflectivities are modified by multiplying the Kirchhoff (small-scale) scattering factor and then large-scale roughness is treated as an added factor for modifying Fresnel reflectivities. The ocean surface emissivity in the FASTEM is written as

$$E_p = E_{F,p}F_c + \left(1 - R_pK + \Delta R_p\right)\left(1 - F_c\right) + \Delta E_\varphi, \qquad (1)$$

where E_p and $E_{F,p}$ denote the ocean surface effective emissivity and the foam emissivity at polarization p, respectively; R_p represents the p-polarized Fresnel reflectivity; ΔR_p is an

Denotes content that is immediately available upon publication as open access.

Corresponding author: Dr. Sang-Moo Lee, dr.sangmoolee@gmail.com, sang-moo.lee@colorado.edu

DOI: 10.1175/JTECH-D-20-0065.1

added reflectivity component by large-scale surface roughness; and F_c indicates the foam fraction; ΔE_φ is the wind direction influences on E_p and is a function of the relative azimuthal angle φ between wind direction and radiometer look. Kirchhoff's bistatic scattering factor K is defined as

$$K = \exp\left(-4k^2\sigma^2\cos^2\theta_{\mathrm{SZA}}\right), \tag{2}$$

where σ is the small-scale surface roughness [i.e., small-scale root-mean-square (rms) height], k is the electromagnetic wavenumber, and θ_{SZA} is the satellite zenith angle. One caveat of this formulation for K is to consider the coherent scattering only, neglecting the incoherent scattering part.

Although the coefficients K and ΔR_p in FASTEM are empirically determined by fitting Eq. (1) to the rigorous two-scale model results, the fitting itself may cause errors in the emissivity calculation. It is because Eq. (1) considers the small- and large-scale roughness separately, not allowing the interactions between the small- and large-scale roughness. In other words, in FASTEM, the small-scale surface scattering occurs over a smooth surface [represented by satellite zenith angle (SZA)] rather than over a geometrically slanted surface [represented by local incidence angle (LIA)]. The FASTEM uses SZA instead of LIA to calculate small-scale surface scattering. Thus, for the better emissivity calculation, the model equation needs to allow interactions between the small- and large-scale roughness, in addition to the use of LIA instead of SZA in Eq. (2), even if the model equation fits into rigorous two-scale model results.

In this study, we attempt to solve the problem inherent in the FASTEM equation by proposing a new concept that the large-scale roughness can be expressed as a function of the LIA within the context of Fresnel reflection theory, incorporating the interactions between the small- and large-scale roughness into the fast ocean surface emissivity model, as done in the two-scale approach. Here the fast ocean surface emissivity model is used as a general term for expressing the fast calculation model for the ocean surface emissivity. With the new expression of the large-scale roughness, we provide a more physically orientated form of the equation for the fast ocean surface emissivity calculation that includes the small-scale scattering over a geometrically rough surface (i.e., the Kirchhoff scattering factor K is expressed as a function of the LIA instead of the SZA). In addition, an algorithm for estimating two-scale roughness from the measured or modeled polarized emissivities in conjunction with the proposed fast ocean surface emissivity equation is provided. In this paper, we will demonstrate that the interactions between two-scale roughness should be considered in order to estimate accurate two-scale roughness influences on the ocean surface emissivity.

2. A new equation for fast ocean surface emissivity calculation

As discussed, the rough surface of the ocean is made up of slanted surfaces that deviated from a flat surface, resulting in LIA value different from the SZA value. Thus, if the SZA is used for the simulation of the emissivities over a target with a rough surface, an error will likely arise due to the incidence angle difference between the flat and slanted surfaces (Sasaki et al. 1987). In addition, the large-scale roughness is also responsible for the small-scale roughness variation because small-scale waves always ride atop large gravity ocean waves. Interactions between small-scale and large-scale roughness are well described in the two-scale model, which has been recognized as the best model to estimate physical seawater emissivity over microwave frequencies (Yueh et al. 1994; Yueh 1997). On the other hand, FASTEM assumes small-scale waves completely separated from large-scale ocean waves, indicating that small-scale bistatic scattering is considered to be on the flat surface. For example, if the large-scale surface roughness brings about 3° of incidence angle changed from 55° (typical SZA of conical scanning radiometer), this assumption induces about 5% difference between bistatic scattering amount with incidence angles of 55° and 55° ± 3°, based on the Eq. (2). Thus, the fast ocean surface emissivity model needs to include interactions between two-scale roughness because the geometric information is not counted for estimating the influences of small-scale roughness on the emissivity, which can become a significant error source.

To improve the roughness problem inherent in Eq. (1), we first define an averaged LIA value as the large-scale surface roughness. To find the mean of the LIA values, the isotropic geometric optics model is employed, in which the effective surface reflectivity can be obtained by using the Gaussian slope distribution to integrate the reflectivities over an infinite number of specular facet (Petty and Katsaros 1994; Phalippou 1996; Wu and Smith 1997). Then the mean emissivity $\overline{E_p}$ and reflectivity $\overline{R_p}$ can be expressed as

$$\overline{E_p} = 1 - \overline{R_p} = 1 - \frac{\int_{-\infty}^{\infty}\int_{-\infty}^{\infty} R_{F,p}(\theta_{\mathrm{LIA}})P\left(dz_x, dz_y\right)Q\,dz_x\,dz_y}{\int_{-\infty}^{\infty}\int_{-\infty}^{\infty} P\left(dz_x, dz_y\right)Q\,dz_x\,dz_y}, \tag{3}$$

where θ_{LIA} is the local incidence angle, which is a function of the slope elements dz_x and dz_y in the x and y directions, respectively; P is the Gaussian probability density function; and Q is a factor related to the roughness and consists of two parts: the area projection factor, defined as the ratio of the inclined and plane facets, and the illumination function, expressing the effects of shadows from adjacent facets.

In this study, we employ further assumption proposed by Stroeve et al. (2006) and Lee et al. (2018a) that the integrated value of reflectivities at each LIA [left-hand side of Eq. (3)] is approximated by the reflectivity at mean LIA value of all local facets [right-hand side of Eq. (3)]; i.e.,

$$\begin{aligned}\int_{-\infty}^{\infty}\int_{-\infty}^{\infty} R_{F,p}(\theta_{\mathrm{LIA}})P\left(dz_x, dz_y\right)Q\,dz_x\,dz_y \\ \approx \overline{R_{F,p}}\left(\overline{\theta_{\mathrm{LIA}}}\right)\int_{-\infty}^{\infty}\int_{-\infty}^{\infty} P\left(dz_x, dz_y\right)Q\,dz_x\,dz_y.\end{aligned} \tag{4}$$

By combining Eq. (3) with Eq. (4), the mean ocean surface reflectivity can be expressed as the mean Fresnel reflectivity modified by the surface roughness at the mean LIA:

$$\overline{R_p} \approx \overline{R_{F,p}}\left(\overline{\theta_{\mathrm{LIA}}}\right). \tag{5}$$

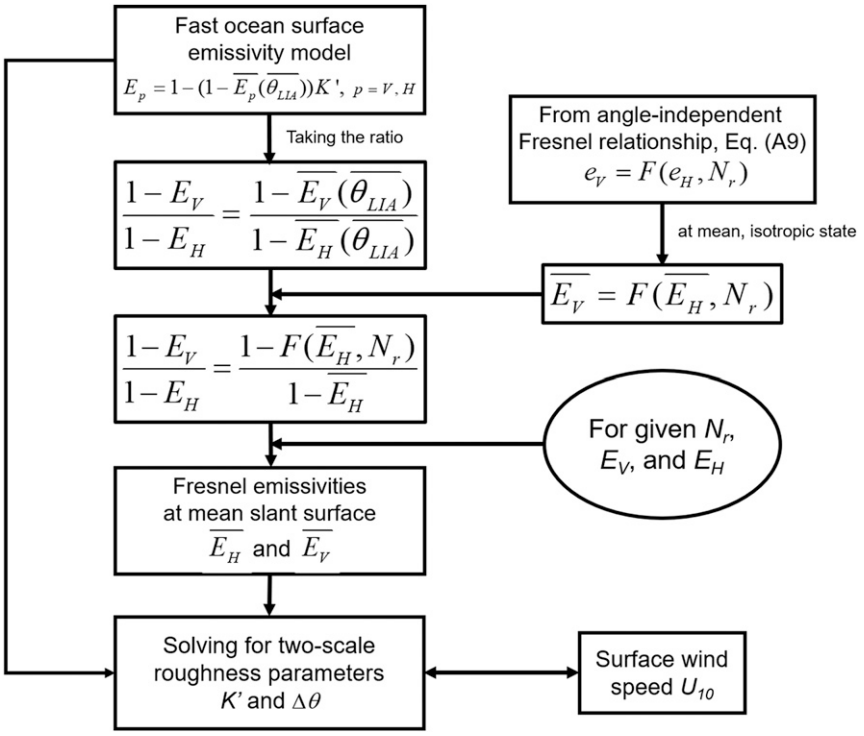

FIG. 1. Flowchart for solving two-scale roughness from the proposed fast ocean surface emissivity equation in conjunction with the combined Fresnel equation.

Compared to the description of large-scale roughness in Eq. (1), $\overline{R_p}$ is now directly described by Fresnel reflection theory but with mean LIA instead of SZA. Equation (5) can allow to interlink between small-scale and large-scale roughness because large-scale roughness is now represented by mean LIA. Therefore, Kirchhoff's approximation over the geometrically rough surface can be written as

$$K' = \exp\left(-4k^2\sigma^2\cos^2\overline{\theta_{\mathrm{LIA}}}\right), \tag{6}$$

where K' is the coherent part of the Kirchhoff's scattering power with mean LIA. At this point, we propose an alternative form of Eq. (1), by mimicking the way employed by the two-scale approximation method and by allowing the small-scale waves to travel over the large-scale titled facets with the mean LIA values ($\overline{\theta_{\mathrm{LIA}}}$). Compared to the FASTEM model, the proposed description does allow the interactions between small-scale and large-scale waves. That is, the seawater reflectivity is affected by small-scale scattering over a geometrically rough surface, rather than over a smooth surface; i.e.,

$$E_p = E_{F,p}F_c + \left(1-\overline{R_{F,p}}K'\right)(1-F_c) + \Delta E_\varphi, \tag{7}$$

where $\overline{R_{F,p}}$ is the mean reflectivity over the geometrically slanted surface defined by Eqs. (4) and (5). In Eq. (7), K' introduces the bistatic scattering applied over the slant surface (represented by LIA) rather than over the flat surface (represented by SZA). As $\overline{R_{F,p}}$ in Eq. (7) is the Fresnel reflection at the mean LIA, the large-scale surface roughness is now directly dealt with Fresnel equations, allowing the interactions between small-scale and large-scale roughness.

3. Examination of two-scale roughness from the proposed model

Here we examine properties of small-scale (K') and large-scale roughness ($\overline{\theta_{\mathrm{LIA}}}$) in the proposed Eq. (7). In so doing, K' and $\overline{\theta_{\mathrm{LIA}}}$ are diagnosed from surface emissivities (from either observations or model results), instead of directly calculating from two-scale model results.

a. Solving method for two-scale roughness

In this subsection, we present how K' and $\overline{\theta_{\mathrm{LIA}}}$ can be diagnosed from given polarized emissivities, with help from a combined Fresnel equation (see appendix A). The solving procedures are summarized in Fig. 1. To determine two-scale roughness, the foam and wind direction effects are omitted for simplicity. Then Eq. (7) becomes

$$E_p = 1-\overline{R_p}(\overline{\theta_{\mathrm{LIA}}})K' = 1-\left[1-\overline{E_p}(\overline{\theta_{\mathrm{LIA}}})\right]K'. \tag{8}$$

Alternatively,

$$1-E_p = \left[1-\overline{E_p}(\overline{\theta_{\mathrm{LIA}}})\right]K'. \tag{9}$$

Over a flat Fresnel surface, the SZA is equal to the LIA (i.e., $\theta_{\mathrm{SZA}} = \overline{\theta_{\mathrm{LIA}}}$) and $K' = 1$, so that Eqs. (8) and (9) can be directly used for calculating the emissivity without relying upon the roughness parameterization. On the other hand, over the

rough surface, which is slanted due to wind stress, SZA is different from LIA, causing an error propagation into the emissivity calculation [Eq. (8)] if SZA is used (Wentz 1992). Here, we define an index of the large-scale roughness as the difference between SZA and LIA (hereafter referred to as $\Delta\theta$ = SZA − LIA) since it represents surface slope deviating from a flat surface.

Estimating K' and $\Delta\theta$, we take the ratio between two polarized emissivities in Eq. (9); i.e.,

$$\frac{1-E_V}{1-E_H}=\frac{1-\overline{E_V}(\overline{\theta_{\mathrm{LIA}}})}{1-\overline{E_H}(\overline{\theta_{\mathrm{LIA}}})}, \tag{10}$$

where subscripts V and H denote the vertical and horizontal polarizations, respectively. In Eq. (10), the bistatic scattering factor has been eliminated. To solve Eq. (10), the mean LIA should be known, which is difficult to obtain without a geometric model in conjunction with the ocean wave height spectrum at a certain sea state. Avoiding this problem, we introduce an angle-independent combined Fresnel relationship which interlinks between two polarized reflectivities without specifying the incidence angle (so-called angle-independent combined Fresnel relationship—see appendix A).

According to the angle-independent combined Fresnel relationship, one component $e_V(\theta)$ (or $e_H(\theta)$) can be expressed by the other component $e_H(\theta)$ (or $e_V(\theta)$) and refractive index (N_r), i.e., $e_V = F(e_H, N_r)$ where e_V and e_H are Fresnel polarized emissivity at vertical and horizontal polarizations, respectively; N_r is adjusted real refractive index; F represents a function defined in Eq. (A9). Thus, if N_r is known, one of two components can be eliminated in equations including Fresnel relationships. By applying this angle-independent combined Fresnel relationship into the mean and isotropic states, i.e.,

$$\frac{1-E_V}{1-E_H}=\frac{1-F(\overline{E_H},N_r)}{1-\overline{E_H}}. \tag{11}$$

Note that only one mean emissivity component remains on the right-hand side beside N_r. The refractive index N_r (or dielectric constant) for seawater can be calculable with high accuracy from a double Debye equation (Meissner and Wentz 2004; Liu et al. 2011) (see appendix B). If we assume that N_r is known, it is now possible to determine $\overline{E_H}$ from given effective sea surface polarized emissivities [i.e., E_V and E_H: left-hand side of Eq. (11)]. Once $\overline{E_H}$ is obtained, $\overline{E_V}$ can be determined since one component can be expressed by another component in the angle-independent combined Fresnel equation. Then K' can be determined from Eq. (8) and the mean LIA from Eq. (A5). Since the SZA is known quantity, $\Delta\theta$ (i.e., SZA − LIA) can be determined for given $\overline{E_V}$, $\overline{E_H}$, and N_r.

b. Roughness parameters from FASTEM simulations

Although we intend to improve the method employed in FASTEM, FASTEM-generated polarized emissivities are used as a reference. It is because, from the use of simulated emissivities, we can examine how the solving method works and furthermore examine whether obtained solutions (here K' and $\Delta\theta$) are consistent with known features related to surface roughness. In this simulation framework, the viewing angle of 55°, which is a typical SZA of satellite-borne conical scanning sensors such as Advanced Microwave Scanning Radiometer (AMSR), is selected and sea surface salinity is fixed at 35 ppt. The sea surface temperature (SST) and wind speed at 10 m above the sea surface for 1 May 2015, obtained from the European Centre for Medium-Range Weather Forecasts interim reanalysis (ERA-Interim) (Dee et al. 2011), are used as inputs for the FASTEM simulation. The model assumes that the clouds and atmospheric moisture and precipitation have been removed. Following the solving method given in section 3a, K' and $\Delta\theta$ are estimated from FASTEM-simulated polarized emissivities and N_r from a dielectric constant module [Eq. (B1) in appendix B].

Estimated K' at 18.7 GHz are given in Fig. 2a. It is noted that lower K' values correspond to regions with low wind speed, such as the Southern Ocean (also see Fig. 2c), consistent with the expectation that the corresponding small-scale scattering increases when the sea surface gravity–capillary waves are enhanced by high winds. It is natural to relate $\Delta\theta$ to the wind speed because the difference between SZA and LIA (i.e., the large-scale roughness) should be proportional to the surface wind speed. To examine such a relationship, the estimated $\Delta\theta$ at 18.7 GHz (Fig. 2b) is compared with the ERA-Interim wind speed at 10 m above the sea surface (U_{10}) over the global ocean (Fig. 2c). It is clearly seen that there is a strong correlation between the two variables. The strong correlation is not surprising because the wind-roughened ocean surface emissivity at a given frequency can be written in terms of the seawater dielectric constant and surface wind speed. Since the dielectric constant of the seawater is related to the foam emissivity, not to the two-scale roughness, the ocean surface emissivity variation due to two-scale roughness should be well expressed by surface wind alone. It is noted that the maximum difference between SZA and LIA is up to 1.5°, corresponding to emissivity uncertainties of 0.017 for E_V and 0.012 for E_H when SZA is used for the emissivity calculation instead of LIA. Given a sea surface temperature of 290 K, such a difference in emissivity corresponds to a brightness temperature difference of about 4 K.

It is worthwhile to examine how significant the influence of interactions between two-scale roughness on the emissivity might be. It is done by estimating Kirchhoff's factor from the same proposed method but not allowing interactions between two-scale roughness, and by comparing the results with ones with interactions allowed. It is accomplished by fixing the incidence angle as SZA (hereafter, Kirchhoff's factor with SZA is called to K''). The percentage difference between K' and K'' is provided in Fig. 3. It is shown that the mean percentage difference between K' and K'' is about 2.1% at 18.7 GHz, suggesting that the interactions between two-scale roughness are considered significant. Notably the maximum difference of 6.1% is found over high wind areas such as Southern Hemispheric midlatitude oceans, which corresponds to 10.6 K difference in brightness temperature at vertical polarization at 290 K of SST.

c. Physical features of estimated roughness parameters

Encouraged by the obtained results from FASTEM simulations, which are found to be consistent with expected meteorological

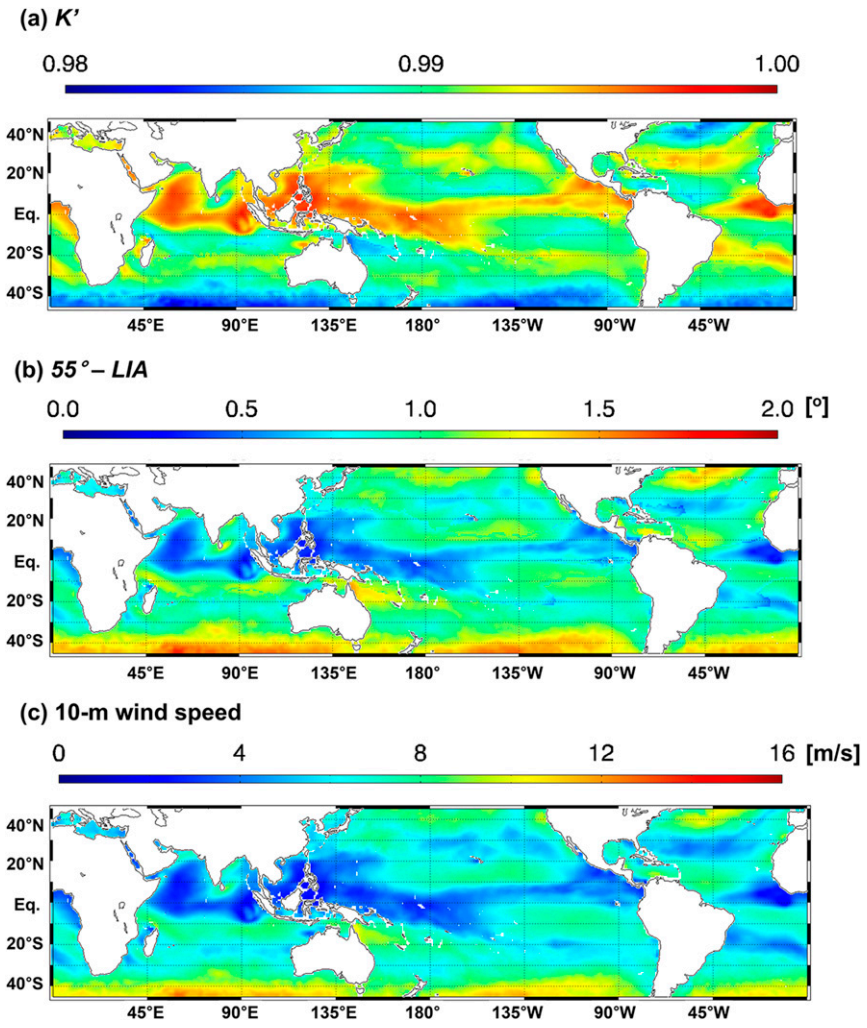

FIG. 2. Geographical distributions of (a) the estimated Kirchhoff scattering factor (K') at 18.7 GHz, (b) difference between SZA of 55° and the estimated LIA, and (c) ERA-Interim wind speed 10 m above the ocean surface.

features, we further examine how the proposed method may be used for providing a more scientific background in emissivity modeling. Here, K' and $\Delta\theta$ are estimated from WindSat- and SSM/I-based emissivity data at five different frequencies of 6.8, 10.7, 18.7, 37.0, and 85.5 GHz. And then the obtained K' and $\Delta\theta$ are compared with U_{10}. In doing so, the procedures shown in Fig. 1 are repeated, now with surface emissivity data from WindSat and SSM/I brightness temperature measurements (Meissner and Wentz 2012, hereafter emissivity data are referred to as MW12).

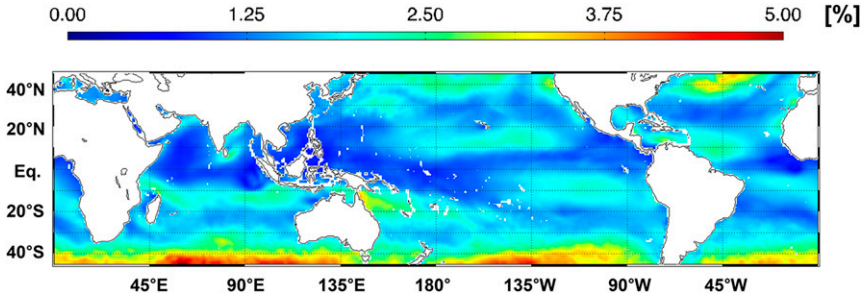

FIG. 3. Geographical distributions of the percentage difference between K' and K'' at 18.7 GHz.

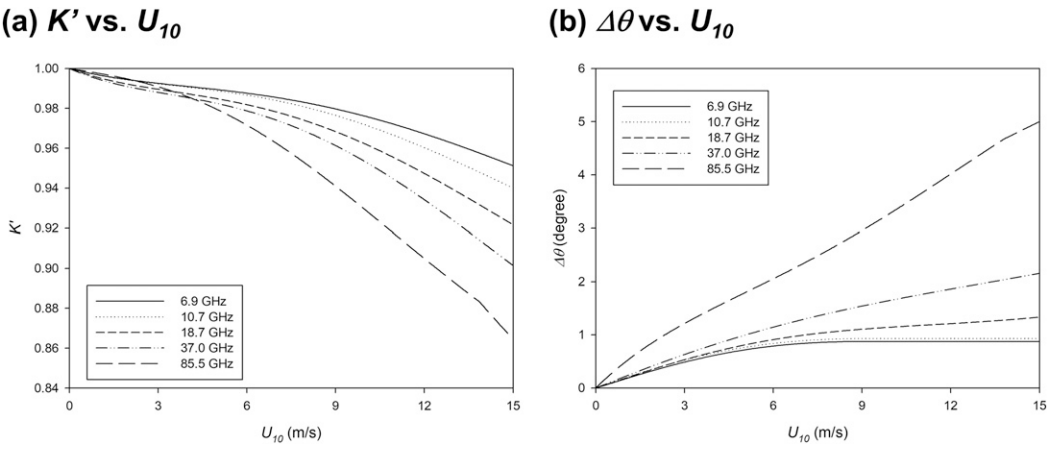

FIG. 4. Relationships (a) between K' and U_{10} and (b) between $\Delta\theta$ and U_{10} for frequencies of 6.8 (solid line), 10.7 (dotted line), 18.7 (dashed line), 37.0 (dashed–dotted line), and 85.5 GHz (long-dashed line).

The MW12 is composed of Fresnel emissivity $E_{F,p}$, isotropic wind-induced emissivity variation ΔE_W (i.e., small-scale and large-scale roughness), and wind direction signal ΔE_φ. It is based on four-year analysis of calibrated brightness temperatures from WindSat and SSM/I, aided with the ocean surface wind stress data from WindSat, QuikSCAT, and National Centers for Environmental Prediction (NCEP) Global Data Assimilation System (GDAS) (Meissner and Wentz 2012). In MW12, $E_{F,p}$, the largest component, is estimated from the Fresnel reflection theory with the dielectric constant of seawater from Meissner and Wentz (2004) model. By summing satellite-measured E_p over all possible wind directions to drop out the azimuthal variation with a harmonic function of φ, the isotropic part of ΔE_W is estimated. Once ΔE_W is known, ΔE_W at a certain φ can be calculable by analyzing the residual as a function of φ and U_{10}. The environments for those emissivities are 55.2° of SZA and 20°C of SST. Since this study focuses on the influence of isotropic roughness (i.e., small-scale and large-scale roughness) on the ocean emissivity, the wind direction signal ΔE_φ is not considered. Thus, effective emissivity E_p can be calculated as follows:

$$E_p = E_{F,p} + \Delta E_W . \tag{12}$$

From the MW12 emissivity data, two-scale roughness are estimated using the procedures described in Fig. 1.

The K' and $\Delta\theta$ estimated from MW12 at 6.8, 10.7, 18.7, 37.0, and 85.5 GHz are now related to the wind speed at 10 m. We limit the wind speed to 15 m s^{-1} in order to exclude the influence of foam on the emissivity (Meissner and Wentz 2012). The relationships between K' and U_{10}, and between $\Delta\theta$ and U_{10} obtained from E_p estimated from MW12 are plotted in Fig. 4. It is shown that K' and $\Delta\theta$ are unity and zero, respectively, in case of the calm sea surface, which is consistent with the theoretical expectation because gravity and capillary waves do not exist without wind.

As U_{10} increases, the impacts of the small- and large-scale roughness become larger. For a wind speed lower than 3 m s^{-1}, the estimated K' is between 0.99 and 1.0, regardless of frequency, indicating that the small-scale roughness at best changes 1% of the Fresnel reflectivity. As wind speed increases, the small-scale roughness becomes larger. On the other hand, the $\Delta\theta$ is between 0.5° and 1.0° for a wind speed lower than 3 m s^{-1}, corresponding to a 1.5%–3% change in the Fresnel reflectivity. When the wind becomes stronger, the general trend in $\Delta\theta$ change seems to depend on the frequency. For instance, $\Delta\theta$ change at 6.8 and 10.7 GHz tends to level off when the wind speed is higher than 8 and 8.5 m s^{-1}, converging to 0.87° and 0.93°, respectively. Similar patterns were observed in the curvature spectrum of the ocean slope distribution, in which the rms curvature of a wind-driven ocean surface tends to saturate as wind speed become higher (Apel 1994; Kunkee and Gasiewski 1997; Elfouhaily et al. 1997). In contrast, the change in $\Delta\theta$ at other frequencies is generally increasing as the wind speed increases. However, the $\partial(\Delta\theta)/\partial(U_{10})$ become smaller as wind speed increases, indicating that the $\Delta\theta$ becomes eventually saturated at a certain wind speed stronger than 10 m s^{-1}. This physical pattern of ocean surface slope distribution is not observed in the large-scale correction term (i.e., ΔR_p) of FASTEM parameterization (Fig. 5).

4. Summary and discussion

In this study, we propose a more physically orientated fast microwave ocean surface emissivity model with new expressions of the small- and large-scale roughness effects on the ocean surface emissivity. A form of the large-scale roughness is devised and proposed in terms of the mean local incidence angle. The theoretical background of this scheme is that the incidence angle likely differs from the satellite zenith angle due to the large-scale ocean surface slope. By incorporating the new form of the roughness effect, the ocean surface emissivity can be modeled as a Fresnel emissivity over a slant slope and then scaled by the Kirchhoff scattering factor.

To evaluate the proposed ocean surface emissivity model, we developed a method to estimate small- and large-scale roughness from two-polarized emissivities (which can be

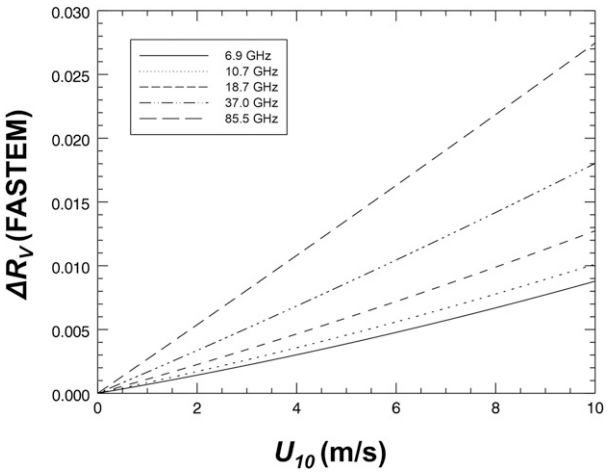

FIG. 5. As in Fig. 4, but for the relationship between ΔR_p from FASTEM and U_{10}.

both modeled and observed values), in conjunction with the angle-independent combined Fresnel equation. We applied this method over a wind-roughened ocean surface, in a simulation framework based on microwave emissivity calculated by FASTEM in the ERA-Interim environment. It was assumed that the clouds and atmospheric moisture and precipitation have been removed. It has been found that the two-scale roughness from the proposed fast ocean surface emissivity equation are closely associated with surface wind speed. It was further demonstrated that the interactions between two-scale roughness should be counted in order to estimate accurate two-scale roughness influences on the ocean surface emissivity. Notably the maximum difference of 6.1% in Kirchhoff's scattering factor between geometrically slanted surface and flat surface is found over high wind areas, which corresponds to 10.6 K difference in brightness temperature at vertical polarization.

Furthermore, based on the MW12 emissivity data from WindSat and SSM/I brightness temperature, the two-scale roughness are estimated using the proposed method described in Fig. 1. For lower wind speed than $3\,\mathrm{m\,s^{-1}}$, the influence of small-scale roughness on the ocean surface emissivity is negligible regardless of frequency. On the other hand, large-scale roughness (i.e., $\Delta\theta$) influences on the emissivity is significant even in the lower wind speed condition. It is interestingly notable that $\Delta\theta$ tends to level off when the wind speed become strong, which is consistent with the observation that the curvature spectrum of a wind-driven ocean surface tends to saturate at a certain high wind speed. This physical pattern of ocean surface wave slope distribution is not observed in the FASTEM-deployed large-scale roughness correction term.

One can employ the proposed method for improving the FASTEM model, which is widely used in data assimilation for weather forecasting. It may be possible because the polarized emissivities from the rigorous two-scale model and/or satellite observation can provide small-scale and large-scale roughness (i.e., K' and $\Delta\theta$), and those two terms can be closely linked to surface wind. Thus, similar to the FASTEM fitting of roughness parameters with known meteorological variables, obtained K' and $\Delta\theta$ can be fitted to the surface wind for the model use. Although such a study is interesting, it seems beyond the targets that this paper is aiming at. We mainly focused on the theoretical development of the model which can allow interactions between small- and large-scale roughness, and on interpreting obtained roughness parameters in terms of physical reasoning.

In doing so, emissivity estimates from well-calibrated satellite measurements are necessary. The Global Precipitation Mission (GPM) Microwave Imager (GMI) measurements are considered to be ideal because the GMI sensor is known to be the well-calibrated passive microwave imager (Berg et al. 2018). Furthermore, for the possible applications for data assimilation in numerical weather forecasting, fittings should cover various frequencies and viewing geometries employed by different microwave sensors. In particular, for cross-tracking sensors such as Advanced Technology Microwave Sounder (AMSU), fittings should be available to cover the full range of scan geometry.

Acknowledgments. The authors thank two anonymous reviewers for their constructive and valuable comments that led to an improved research article. They would also like to thank the Numerical Weather Prediction Satellite Application Facility (NWP SAF) for Fast Microwave Emissivity Model (FASTEM) version 5 and ECMWF for ocean surface properties. This research has been supported by National Research Foundation of Korea (NRF) grant funded by the Korean government (MSIP) (NRF-2016R1A2B4009551 and NRF-2019R1A6A3A03032352). BJS was also supported by NRF-2018M1A3A3A02065661.

APPENDIX A

Angle-Independent Combined Fresnel Relationship

Here we derive theoretical Fresnel equations that are independent of the LIA. Fresnel reflection theory describes the polarized light reflection at a smooth interface between two isotropic media. The polarized reflectivities over a Fresnel surface can be expressed in terms of the refractive index and LIA (θ) as follows:

$$R_V = \left| \frac{N_r^2 \cos\theta - \sqrt{N_r^2 - \sin^2\theta}}{N_r^2 \cos\theta + \sqrt{N_r^2 - \sin^2\theta}} \right|^2, \tag{A1}$$

$$R_H = \left| \frac{\cos\theta - \sqrt{N_r^2 - \sin^2\theta}}{\cos\theta + \sqrt{N_r^2 - \sin^2\theta}} \right|^2, \tag{A2}$$

where R_V and R_H are the vertically and horizontally polarized reflectivities, respectively, and N_r is the relative adjusted real refractive index between two media, which can be expressed in terms of the real (n_r) and imaginary (n_i) parts of the complex refractive index (Liou 2002).

Fresnel theory has been used in the analysis of Earth-surface observations and radiative transfer modeling, because it can be used to determine the surface emissivity of a target if N_r and θ are given (Hewison and English 1999; Weng et al. 2001; Escorihuela et al. 2007; Kerr et al. 2012; Lee and Sohn 2015).

Nevertheless, there seems to be a limitation in the direct application of Fresnel theory into satellite observations because a priori information about the dielectric properties of the material of interest is limited. However, the following relations may be used to expand the application of Fresnel theory to surface remote sensing problems. Sohn and Lee (2013) derived an analytical relationship between N_r and R_H after rearranging Eq. (A2), as follows:

$$N_r = \sqrt{1 + \frac{4R_H^{1/2}\cos^2\theta}{(R_H^{1/2} - 1)^2}}. \tag{A3}$$

Next, by combining Eqs. (A3) and (A1), the relationship between the Fresnel reflectivities (so-called combined Fresnel equation), in which the refractive index has been eliminated, is derived:

$$R_V = R_H^2\left(\frac{1 + R_H^{-1/2}\cos 2\theta}{1 + R_H^{1/2}\cos 2\theta}\right)^2. \tag{A4}$$

It is now possible to use Fresnel theory to study smooth targets using satellite remote sensing data without a priori knowledge of the refractive indices of the materials involved. In practice, Eq. (A4) has been utilized to study soil moisture, polar sea ice, etc., using spaceborne microwave measurements (Lee and Sohn 2015; Zhu et al. 2016; Sun et al. 2017; Lee et al. 2018a,b). In the case of a geometrically rough surface, however, the reliability of satellite-based applications using Eq. (A4) is limited, because the SZA is generally different from the LIA. But these limitations can be avoided if there exists a relationship between the Fresnel reflectivities that is independent of the LIA and if N_r is known, e.g., in the case of water or bare soil. In this study, we derive an angle-independent relationship between the Fresnel polarized reflectivities and use it to estimate the surface roughness.

When θ is acute, Eq. (A3) can be written as

$$\cos\theta = \frac{(N_r^2 - 1)^{1/2}(1 - R_H^{1/2})}{2R_H^{1/4}}. \tag{A5}$$

From Eq. (A5), $N_r^2\cos\theta$ and $\sqrt{N_r^2 - \sin^2\theta}$ contained in Eq. (A1) can be thus expressed as follows:

$$N_r^2\cos\theta = \frac{N_r^2(N_r^2 - 1)^{1/2}(1 - R_H^{1/2})}{2R_H^{1/4}}, \tag{A6}$$

$$\sqrt{N_r^2 - \sin^2\theta} = \frac{(N_r^2 - 1)^{1/2}(1 + R_H^{1/2})}{2R_H^{1/4}}. \tag{A7}$$

By inserting Eqs. (A6) and (A7) into Eq. (A1), R_V can be expressed in terms of R_H and N_r as follows:

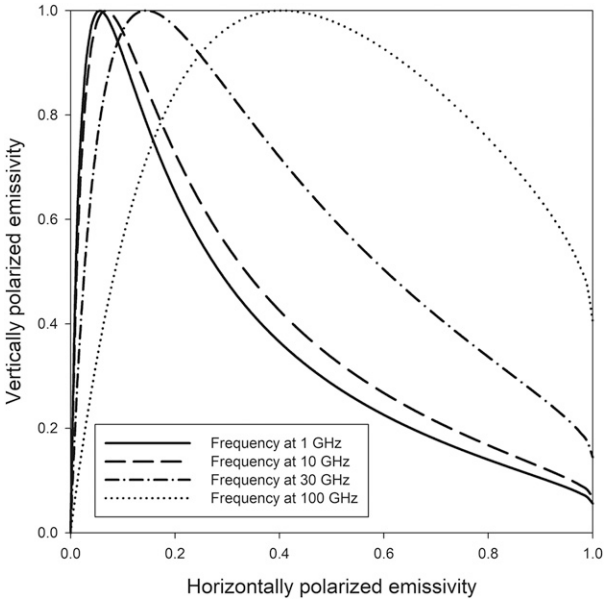

FIG. A1. Relationship between horizontally (x axis) and vertically (y axis) polarized emissivities of the saline water for frequencies of 1 (solid line), 10 (long-dashed line), 30 (dashed–dotted line), and 100 GHz (dotted line).

$$R_V = \left[\frac{(N_r^2 - 1) - R_H^{1/2}(N_r^2 + 1)}{(N_r^2 + 1) - R_H^{1/2}(N_r^2 - 1)}\right]^2. \tag{A8}$$

Then, by allowing the energy conservation, Eq. (A8) can be written as

$$e_V = 1 - \left[\frac{(N_r^2 - 1) - (1 - e_H)^{1/2}(N_r^2 + 1)}{(N_r^2 + 1) - (1 - e_H)^{1/2}(N_r^2 - 1)}\right]^2 = F(e_H, N_r), \tag{A9}$$

where e_V and e_H are the vertically and horizontally polarized surface emissivities, respectively, over the smooth surface. From Eq. (A9), one finds that F is a function of e_H and N_r but not θ. Using Eq. (A9), one component of the polarized emissivity can be expressed in terms of the other component for a given N_r.

Thus, once N_r of the target of interest is known, one may use Eq. (A9) to determine the relationship between e_H and e_V without knowledge of the LIA. However, by studying the relationship between e_H and e_V at four different frequencies (Fig. A1), one discovers that two e_H solutions are possible for every e_V. Fortunately, if the LIA is smaller than Brewster's angle over the ocean, the smaller of the two solutions is the desired one. Since the two e_H solutions approach one other as the frequency decreases, care should be taken when selecting the final e_H solution at low microwave frequencies.

APPENDIX B

Dielectric Constant Model for Seawater

When an electric field is incident upon the water surface, polarization occurs due to charge separation and molecular

rearrangement within the water (Liu et al. 2011). This polarization is mainly described by the dielectric constant (i.e., refractive index) of the water. The complex dielectric constant ε is an essential parameter for describing surface emission and absorption of the material. For seawater, Klein and Swift's model had been widely used (Klein and Swift 1977). It uses a single Debye relaxation law to fit the dielectric constant with respect to frequency f, temperature T_s, and salinity S. But Klein and Swift's model gets inaccurate as the frequency increases because of the ignore of intermolecular interaction (Guillou et al. 1998). To consider the intermolecular interaction within the water, a double Debye relaxation model has been introduced and widely adopted:

$$\varepsilon(T_s,S)=\frac{\varepsilon_s(T_s,S)-\varepsilon_1(T_s,S)}{1+i[f/f_1(T_s,S)]}+\frac{\varepsilon_1(T_s,S)-\varepsilon_\infty(T_s,S)}{1+i[f/f_2(T_s,S)]}+\varepsilon_\infty(T_s,S)-i\frac{\alpha(T_s,S)}{(2\pi\varepsilon_0)f}, \tag{B1}$$

where ε_s, ε_1, and ε_∞ are the dielectric constants at a static frequency, intermediate frequency, and infinite frequency, respectively; ε_0 is the permittivity of free space, which is 8.8429×10^{-12} F m^{-1}; f_1 and f_2 are the relaxation frequency constants at between static and intermediate frequencies and between intermediate and infinite frequencies, respectively; and α is the ionic conductivity of seawater. Through the double Debye equation, coefficients to estimate each component are determined by fitting the dielectric constant measurements at microwave frequencies. There are invaluable efforts to determine accurate coefficients within the dielectric model (Meissner and Wentz 2004; Liu et al. 2011). Among them, Liu et al. (2011) model has been adopted in this study.

REFERENCES

Anguelova, M. D., 2008: Complex dielectric constant of sea foam at microwave frequencies. *J. Geophys. Res.*, **113**, C08001, https://doi.org/10.1029/2007JC004212.

Apel, J. R., 1994: An improved model of the ocean surface wave vector spectrum and its effects on radar backscatter. *J. Geophys. Res.*, **99**, 16 269–16 291, https://doi.org/10.1029/94JC00846.

Berg, W., R. Kroodsma, C. D. Kummerow, and D. S. McKague, 2018: Fundamental climate data records of microwave brightness temperatures. *Remote Sens.*, **10**, 1306, https://doi.org/10.3390/rs10081306.

Bormann, N., A. Geer, and S. English, 2012: Evaluation of the microwave ocean surface emissivity model FASTEM-5 in the IFS. ECMWF Tech. Memo. 667, 20 pp., https://www.ecmwf.int/node/8303.

Dee, D. P., and Coauthors, 2011: The ERA-Interim reanalysis: Configuration and performance of the data assimilation system. *Quart. J. Roy. Meteor. Soc.*, **137**, 553–597, https://doi.org/10.1002/qj.828.

Elfouhaily, T., B. Chapron, K. Katsaros, and D. Vandemark, 1997: A unified directional spectrum for long and short wind-driven waves. *J. Geophys. Res.*, **102**, 15 781–15 796, https://doi.org/10.1029/97JC00467.

English, S. J., and T. J. Hewison, 1998: A fast generic millimetre-wave emissivity model. *Proc. SPIE*, **3503**, 288–300, https://doi.org/10.1117/12.319490.

Escorihuela, M. J., and Coauthors, 2007: A simple model of the bare soil microwave emission at L-band. *IEEE Trans. Geosci. Remote Sens.*, **45**, 1978–1987, https://doi.org/10.1109/TGRS.2007.894935.

Gasiewski, A. J., and D. B. Kunkee, 1994: Polarized microwave emission from water waves. *Radio Sci.*, **29**, 1449–1466, https://doi.org/10.1029/94RS01923.

Guillou, C., W. J. Ellison, L. Eymard, K. Lamkaouchi, C. Prigent, G. Delbos, A. Balana, and S. A. Boukabara, 1998: Impact of new permittivity measurements on sea-surface emissivity modelling in microwave. *Radio Sci.*, **33**, 649–667, https://doi.org/10.1029/97RS02744.

Hewison, T. J., and S. J. English, 1999: Airborne retrievals of snow and ice surface emissivity at millimeter wavelengths. *IEEE Trans. Geosci. Remote Sens.*, **37**, 1871–1879, https://doi.org/10.1109/36.774700.

Hwang, P., 2012: Foam and roughness effects on passive microwave remote sensing of the ocean. *IEEE Trans. Geosci. Remote Sens.*, **50**, 2978–2985, https://doi.org/10.1109/TGRS.2011.2177666.

Johnson, J. T., 2006: An efficient two-scale model for the computation of thermal emission and atmospheric reflection from the sea surface. *IEEE Trans. Geosci. Remote Sens.*, **44**, 560–568, https://doi.org/10.1109/TGRS.2005.855999.

Kerr, Y. H., and Coauthors, 2012: The SMOS soil moisture retrieval algorithm. *IEEE Trans. Geosci. Remote Sens.*, **50**, 1384–1403, https://doi.org/10.1109/TGRS.2012.2184548.

Klein, L. A., and C. T. Swift, 1977: An improved model for the dielectric constant of sea water at microwave frequencies. *IEEE J. Oceanic Eng.*, **2**, 104–111, https://doi.org/10.1109/JOE.1977.1145319.

Kunkee, D. B., and A. J. Gasiewski, 1997: Simulation of passive microwave wind direction signatures over the ocean using an asymmetric-wave geometrical optics model. *Radio Sci.*, **32**, 59–78, https://doi.org/10.1029/96RS02434.

Lee, S.-M., and B.-J. Sohn, 2015: Retrieving the refractive index, emissivity, and surface temperature of polar sea ice from 6.9 GHz microwave measurements: A theoretical development. *J. Geophys. Res. Atmos.*, **120**, 2293–2305, https://doi.org/10.1002/2014JD022481.

——, ——, and H. Shi, 2018a: Impact of ice surface and volume scatterings on the microwave sea ice apparent emissivity. *J. Geophys. Res. Atmos.*, **123**, 9220–9237, https://doi.org/10.1029/2018JD028688.

——, ——, and C. D. Kummerow, 2018b: Long-term Arctic snow/ice interface temperature from special sensor for microwave imager measurements. *Remote Sens.*, **10**, 1795, https://doi.org/10.3390/rs10111795.

Liou, K., 2002: *An Introduction to Atmospheric Radiation*. 2nd ed. International Geophysics Series, Vol. 84, Academic Press, 583 pp.

Liu, Q., F. Weng, and S. J. English, 2011: An improved fast microwave water emissivity model. *IEEE Trans. Geosci. Remote Sens.*, **49**, 1238–1250, https://doi.org/10.1109/TGRS.2010.2064779.

Meissner, T., and F. J. Wentz, 2004: The complex dielectric constant of pure and sea water from microwave satellite observations. *IEEE Trans. Geosci. Remote Sens.*, **42**, 1836–1849, https://doi.org/10.1109/TGRS.2004.831888.

——, and ——, 2012: The emissivity of the ocean surface between 6 and 90 GHz over a large range of wind speeds and Earth incidence angles. *IEEE Trans. Geosci. Remote Sens.*, **50**, 3004–3026, https://doi.org/10.1109/TGRS.2011.2179662.

Monahan, E. C., and I. G. O'Muircheartaigh, 1986: Whitecaps and the passive remote sensing of the ocean. *Int. J. Remote Sens.*, **7**, 627–642, https://doi.org/10.1080/01431168608954716.

Petty, G. W., and K. B. Katsaros, 1994: The response of the SSM/I to the marine environment. Part II: A parameterization of the effect of sea surface slope distribution on emission and reflection. *J. Atmos. Oceanic Technol.*, **11**, 617–628, https://doi.org/10.1175/1520-0426(1994)011<0617:TROTST>2.0.CO;2.

Phalippou, L., 1996: Variational retrieval of humidity profile, wind speed and cloud liquid-water path with the SSM/I: Potential for numerical weather prediction. *Quart. J. Roy. Meteor. Soc.*, **122**, 327–355, https://doi.org/10.1002/qj.49712253002.

Sasaki, Y., I. Asanuma, K. Muneyama, G. Naito, and T. Suzuki, 1987: The dependence of sea-surface microwave emission on wind speed, frequency, incidence angle, and polarization over the frequency range from 1 to 40 GHz. *IEEE Trans. Geosci. Remote Sens.*, **GE-25**, 138–146, https://doi.org/10.1109/TGRS.1987.289813.

Sohn, B.-J., and S.-M. Lee, 2013: Analytical relationship between polarized reflectivities on the specular surface. *Int. J. Remote Sens.*, **34**, 2368–2374, https://doi.org/10.1080/01431161.2012.744490.

Stogryn, A., 1972: The emissivity of sea foam at microwave frequencies. *J. Geophys. Res.*, **77**, 1658–1666, https://doi.org/10.1029/JC077i009p01658.

Stroeve, J. C., and Coauthors, 2006: Impact of surface roughness on AMSR-E sea ice products. *IEEE Trans. Geosci. Remote Sens.*, **44**, 3103–3117, https://doi.org/10.1109/TGRS.2006.880619.

Sun, X., Y. Liu, X. Yu, H. Wu, and N. Zhang, 2017: Three-dimensional measurement for specular reflection surface based on reflection component separation and priority region filling theory. *Sensors*, **17**, 215, https://doi.org/10.3390/s17010215.

Weng, F., B. Yan, and N. C. Grody, 2001: A microwave land emissivity model. *J. Geophys. Res.*, **106**, 20 115–20 123, https://doi.org/10.1029/2001JD900019.

Wentz, F. J., 1975: A two-scale scattering model for foam-free sea microwave brightness temperature. *J. Geophys. Res.*, **80**, 3441–3446, https://doi.org/10.1029/JC080i024p03441.

——, 1992: Measurement of oceanic wind vector using satellite microwave radiometer. *IEEE Trans. Geosci. Remote Sens.*, **30**, 960–972, https://doi.org/10.1109/36.175331.

Wu, X., and W. L. Smith, 1997: Emissivity of rough sea surface for 8–13 μm: Modeling and verification. *Appl. Opt.*, **36**, 2609–2619, https://doi.org/10.1364/AO.36.002609.

Yueh, S., 1997: Modeling of wind direction signals in polarimetric sea surface brightness temperatures. *IEEE Trans. Geosci. Remote Sens.*, **35**, 1400–1418, https://doi.org/10.1109/36.649793.

——, R. Kwok, F. K. Li, S. V. Nghiem, W. J. Wilson, and J. A. Kong, 1994: Polarimetric passive remote sensing of ocean wind vectors. *Radio Sci.*, **29**, 799–814, https://doi.org/10.1029/94RS00450.

Zhu, B., X. Song, P. Leng, C. Sun, R. Wang, and X. Jiang, 2016: A novel simplified algorithm for bare surface soil moisture retrieval using L-band radiometer. *ISPRS Int. J. Geoinf.*, **5**, 143, https://doi.org/10.3390/ijgi5080143.